A Single Input Single Output Formulation for Yaw Rate and Sideslip Angle Control via Torque-Vectoring

Basilio Lenzo[1], Aldo Sorniotti[2], Patrick Gruber[2]
[1]Department of Engineering and Mathematics, Sheffield Hallam University, S1 1WB Sheffield, UK
[2]Centre for Automotive Engineering, University of Surrey, GU2 7XH Guildford, UK

E-mail: basilio.lenzo@shu.ac.uk

Many torque-vectoring controllers are based on the concurrent control of yaw rate and sideslip angle through complex multi-variable control structures. In general, the target is to continuously track a reference yaw rate, and constrain the sideslip angle to remain within thresholds that are critical for vehicle stability. To achieve this objective, this paper presents a single input single output (SISO) formulation, which varies the reference yaw rate to constrain sideslip angle. The performance of the controller is successfully validated through simulations and experimental tests on an electric vehicle prototype with four drivetrains.

Topics / Vehicle Dynamics and Chassis Control

1. INTRODUCTION

Electric vehicles with individually controlled drivetrains provide significant benefits in terms of active safety and drivability. In fact, they allow the allocation of desired amounts of torque to each driven wheel, i.e., torque-vectoring (TV). TV permits the generation of a direct yaw moment through the controlled left-to-right wheel torque distribution. TV has been widely investigated in the literature. Several studies propose TV-based yaw rate control strategies to improve vehicle handling [1-4], shape the vehicle understeer characteristic, and increase yaw and sideslip damping during transients [5-7]. Vehicle handling is also influenced by the variation of the front-to-rear wheel torque distribution, which is achievable in four-wheel-drive vehicles with TV capability [8-9].

Yaw rate controllers need the generation of a reference yaw rate, requiring a good estimation of the tire-road friction coefficient [10]. TV controllers using a reference yaw rate based on inaccurate friction estimation can lead to dangerous vehicle behavior (see [11-12] for general discussions on the topic). However, prompt friction estimation is still a difficult task. Therefore, the yaw rate controller can be coupled with an appropriate sideslip angle controller, able to provide safe performance at the vehicle cornering limit, even in presence of rather imprecise friction estimation [13].

This paper presents a single input single output (SISO) formulation for concurrent yaw rate and sideslip angle control. The reference yaw rate is varied as a function of the estimated or measured sideslip angle. The formulation is validated via phase-plane simulations and experiments on an electric vehicle prototype.

2. CONTROLLER

The simplified schematic of the vehicle control structure is shown in Fig. 1 [12]. It includes:

- A reference yaw rate generator, consisting of two sub-systems. The "Handling yaw rate generator" defines the so-called handling yaw rate, r_h, which corresponds to a desired vehicle cornering response in steady-state conditions, assuming a certain tire-road friction level. In the "Sideslip-based correction" sub-system, r_h is corrected based on the actual sideslip angle and lateral acceleration, as detailed later.
- A high-level controller, generating the overall traction/braking force and direct yaw moment demands, respectively F_X and M_Z, to achieve the reference vehicle behavior, starting from the outputs of the drivability maps and reference yaw rate generator. In this study M_Z is the output of a proportional integral (PI) controller, such as the one in [6]. However, the proposed formulations and analyses have general validity, and could be implemented with any other SISO control structure.
- A wheel torque allocator, which calculates the reference motor torques, τ_i, and brake pressures, p_i, for each wheel, to generate the values of F_X and M_Z requested by the high-level controller. The total drivetrain torques on the left- and right-hand sides of the vehicle, τ_L and τ_R, are obtained as:

$$\tau_L = 0.5\left(F_X - \frac{M_Z}{d}\right)R_w$$
$$\tau_R = 0.5\left(F_X + \frac{M_Z}{d}\right)R_w \quad (1)$$

where d is the half-track width and R_w is the wheel radius. In this study the wheel torque demands are evenly distributed between the front and rear wheels of the respective side. More advanced control allocation strategies could be adopted [14-15].

However, a simple and predictable control allocation algorithm is ideal for the analysis of this study, focused on the performance of the reference yaw rate generator and high-level controller.

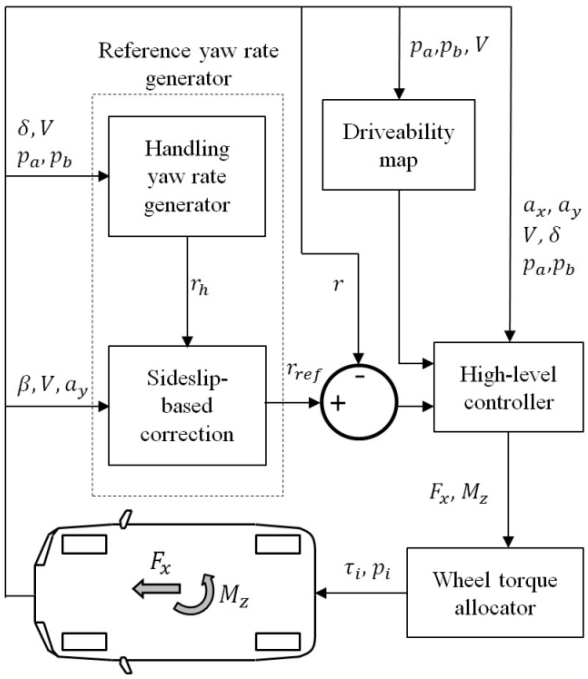

Fig. 1. Simplified control structure schematic (from [12]).

In the proposed formulation, a first order transfer function is adopted to calculate the reference yaw rate, r_{ref}, from its steady-state value, $r_{ref,st}$, which is given by:

$$r_{ref,st} = r_h - F(r_h - K_s r_s) = (1-F)r_h + FK_s r_s \quad (2)$$

where r_h is the handling yaw rate; r_s is the stability yaw rate, i.e., a yaw rate that is compatible with the current cornering conditions of the vehicle, corresponding to the measured lateral acceleration, a_y; and F is a linear function of the absolute value of the sideslip angle, $|\beta|$, saturated between 0 and K_f:

$$F = \begin{cases} 0 & if \quad |\beta| < \beta_{act} \\ \dfrac{|\beta| - \beta_{act}}{\beta_{lim} - \beta_{act}} K_f & if \quad \beta_{act} \le |\beta| \le \beta_{lim} \\ K_f & if \quad |\beta| > \beta_{lim} \end{cases} \quad (3)$$

The sideslip-based correction intervenes only when $|\beta|$ is beyond the activation threshold, β_{act}. This threshold is sufficiently large such that it is not exceeded during the normal operation of the yaw rate controller in high friction conditions. On the other hand, a sideslip angle exceeding β_{act} indicates a too high yaw rate. If $|\beta|$ is above the limit threshold, β_{lim}, the sideslip-based contribution reduces the reference yaw rate to $r_{ref,st} = (1-K_f)r_h + K_f K_s r_s$. For example, if the tuning parameters K_f and K_s are assumed equal to 1, then $r_{ref,st} = r_s$ for high values of sideslip angle. This approach is simpler and easier to tune compared to [16], which also takes into account the sideslip angle rate, $\dot{\beta}$. r_s is calculated from its saturation value, r_{sat}, which is a function of a_y according to the steady-state relationship between yaw rate and a_y [12]:

$$r_{sat} = \frac{a_y - sign(a_y)\Delta a_y}{V} \quad (4)$$

The parameter Δa_y, which varies as a function of a_y, ensures that the vehicle with a yaw rate equal to r_{sat} is actually operating within its cornering limit. r_s is given by:

$$r_s = \begin{cases} r_h & if \quad |r_h| < |r_{sat}| \\ |r_{sat}| sign(r_h) & if \quad |r_h| \ge |r_{sat}| \end{cases} \quad (5)$$

Hence, r_s is the result of the saturation of r_h according to the available tire-road friction conditions, defined by the measured lateral acceleration.

The sideslip angle, β, is conventionally defined as the angle between the velocity of the vehicle center of gravity and the local longitudinal axis, in a top view [17-18]. However, a sideslip angle could be potentially defined for any other point on the longitudinal axis of the vehicle reference system. In Fig. 2 the sideslip angle at the center of gravity is indicated as β_{CG}, and alternative locations are considered. In particular, relevant points are deemed to be the front axle and the rear axle of the vehicle, with the corresponding sideslip angles indicated as β_{FA} and β_{RA}.

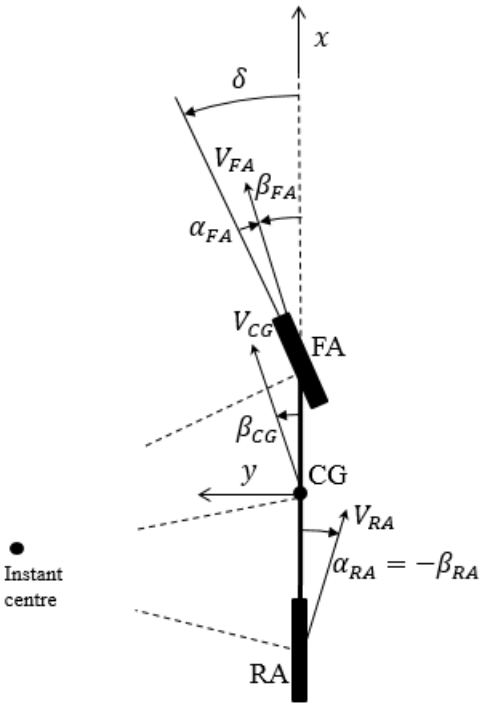

Fig. 2. Top view of a single-track vehicle model with indication of the main parameters and variables.

The sideslip angle consists of two contributions, i.e.: i) a kinematic contribution, related to the trajectory radius at zero tire slip angle; and ii) a dynamic contribution, depending on the actual dynamic condition of the vehicle, associated with tire slip angles. Ideally, only the latter should be the target of the control action, since i) is a geometry-dependent variable. Because of its kinematic contribution, the sideslip angle at the center of gravity can assume rather large values also in non-critical driving conditions, e.g., during low radius steering at low speed. As vehicles do not normally have a rear-wheel steering capability, it follows that β_{RA} does not include any

kinematic contribution and is ideal for vehicle control purposes. Hence, the developed algorithm is applied with β_{RA} in Eq. 3.

The sideslip angle can be either measured or estimated. In this study it was measured by a Datron sensor mounted on the front end of the vehicle (Fig. 4). However, the cost of such a sensor is very high, which justifies the adoption of estimation techniques [19-22]. Once the measurement or estimate of the sideslip angle is available at any point of the vehicle, the sideslip angle at any other point can be easily calculated using the vehicle yaw rate and relevant geometric parameters [17-18].

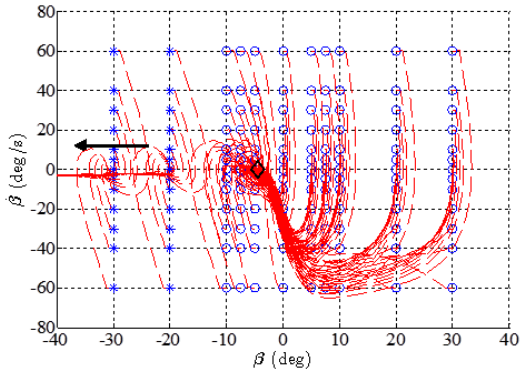

a)

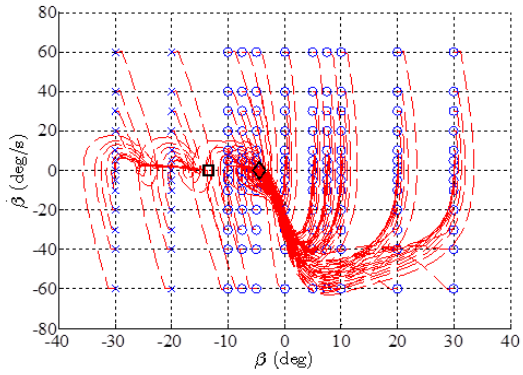

b)

Fig. 3. Phase-plane plots for the controlled vehicle, at 80 km/h, with 50 deg of steering wheel angle. a) TV controller based only on the handling yaw rate; and b) TV controller with the sideslip-based yaw rate correction. *: points that diverge; ○: points that converge regardless of the sideslip-based correction; ×: points that converge to □; ◊: equilibrium of the vehicle in a); □: additional equilibrium of the vehicle in b).

3. SIMULATION RESULTS

A $\dot{\beta}(t)$-$\beta(t)$ phase-plane analysis (where t is time) is carried out with a vehicle simulation model including nonlinear tire behavior and the effect of the load transfers induced by the lateral acceleration. Several combinations of β and $\dot{\beta}$ are imposed as initial conditions for the vehicle simulator, which outputs the evolution of the model states in the time domain [23]. Then these can be represented in the $\dot{\beta}$-β plane, to identify the initial conditions from which the system response converges to an equilibrium.

Fig. 3 reports the simulation results for a high tire-road friction coefficient, at 80 km/h and with a constant 50 deg steering wheel angle (left turn), with two set-ups: a) the vehicle with the TV controller using only the handling yaw rate, i.e., without sideslip-based correction (Fig. 3a)); and b) the vehicle with the TV controller including the sideslip-based correction of the reference yaw rate (Fig. 3b)). The handling yaw rate characteristics are those of the Sport Mode in [5].

Fig. 3a) shows that all the points characterized by an initial value of $\beta \geq$ -10 deg converge to the equilibrium $\beta_{ss} =$ -4.5 deg, while for $\beta <$ -10 deg the system diverges. The benefit of the sideslip-based correction is clearly visible in Fig. 3b), where the system converges regardless of the initial conditions. In particular, in this case there are two equilibria. In Fig. 3b) the originally stable points of Fig. 3a) converge to the same equilibrium as in Fig. 3a). On the other hand, the points originally unstable become stable, and they converge to a different equilibrium at approximately -15 deg, consistent with the values of β_{act} and β_{lim} selected for the specific simulations. In general, it was verified that the tuning parameters Δa_y, K_f and K_s affect the shape of the trajectories, but not the location of the second sideslip angle equilibrium, which is mainly determined by β_{lim}.

In summary, compared to the TV controller only based on the handling yaw rate [5], the proposed sideslip correction brings a significant extension of the stable region of vehicle operation in the $\dot{\beta}$-β plane, even when the handling yaw rate is appropriate for the specific tire-road friction conditions. This positive result encouraged the experimental assessment of the controller formulation.

4. EXPERIMENTAL RESULTS

Experimental tests were conducted on the electric Range Rover Evoque prototype of the European Union funded project iCOMPOSE (Fig. 4). The vehicle includes four on-board electric drivetrains, each of them consisting of a switched reluctance electric motor drive, a single-speed transmission, and a half-shaft with constant velocity joints. The TV controller was implemented on a dSPACE AutoBox system installed on the vehicle.

Fig. 4. The iCOMPOSE electric vehicle demonstrator with the Corrsys Datron sensor installed on the front end.

The proving ground located in Weert (the Netherlands) was used for the experimental tests of this study (Fig. 5). The test area consists of a surface that is 150 m long and 41 m wide. The central part (50 m x 25 m) of such surface is characterized by a low friction area, made of epoxy and kept constantly wet by means of sprinklers. The remaining part of the proving ground is covered with common asphalt, which was dry during the tests. The friction coefficient in the low friction area is ≈15% of the friction coefficient in the high friction area.

A very demanding test maneuver was executed in this

study:

- The car is accelerated on a straight line until a reference speed value, V_m, is steadily achieved.
- Once the vehicle is stabilized on V_m, a constant wheel torque demand (100 Nm) is applied through the dSPACE system, thus bypassing the driver input on the accelerator pedal.
- The vehicle executes a slalom maneuver with cones located at 20 m from each other on a straight line.
- The vehicle starts the test on the high friction area, then enters the low friction area, and, at the end of the maneuver, goes back into the high friction area.
- V_m is defined as the maximum initial speed at which the baseline vehicle (i.e., the vehicle without TV controller) can complete the maneuver without hitting any cone. The value of V_m was determined through multiple tests.

The test maneuver is particularly critical for stability control systems, because of the swift variation of the tire-road friction coefficient, which requires prompt adaptation of the controller. Hence, these test conditions are even more demanding than those typically achievable in a uniformly low-friction proving ground.

Fig. 5. The Weert proving ground (the Netherlands), with the central low friction area and sprinklers on each side.

The maneuver was executed with: i) the baseline vehicle, i.e., without TV controller; ii) the active vehicle with the TV controller only based on r_h, i.e., without sideslip contribution in the definition of the reference yaw rate. The r_h look-up table was tuned for a high value of the tire-road friction coefficient (dry tarmac); and iii) the active vehicle with the proposed SISO yaw rate and sideslip controller, and the same r_h set-up as in ii). Configurations i), ii) and iii) are indicated respectively as B, YO and YS in the remainder.

Fig. 6 reports the time histories of the sideslip angle at the center of gravity and yaw rate for the three set-ups. In particular, the vehicle enters the low friction area at ≈4 s and leaves it at ≈9 s, with some variability caused by the difference in the velocity profiles of the multiple controller configurations along the maneuver. The results show that yaw rate-based TV control on its own can be dangerous if the friction conditions are not well estimated. In fact, the YO vehicle spins at ≈8.5 s, and is more aggressive than the B vehicle, with which the driver manages to complete the maneuver, despite the large peaks of sideslip angle. After 8.5 s, in the YO vehicle the sideslip angle has opposite sign with respect to the yaw rate. The driver countersteers, but this is not sufficient to complete the test. The oversteer problem of the YO vehicle is caused by the excessively high absolute values of the reference (handling) yaw rate, designed for high friction conditions. The response of the YO vehicle is typical of a TV-controlled vehicle without a working friction estimator capable of modifying the reference yaw rate. The important conclusion is that a TV-controlled vehicle that is not properly tuned for low or variable friction conditions is potentially more dangerous than the corresponding baseline vehicle. The proposed sideslip-based correction of the reference yaw rate overcomes this issue. In fact, the YS vehicle adapts to the prevailing friction conditions and safely completes the maneuver, maintaining low values of sideslip angle.

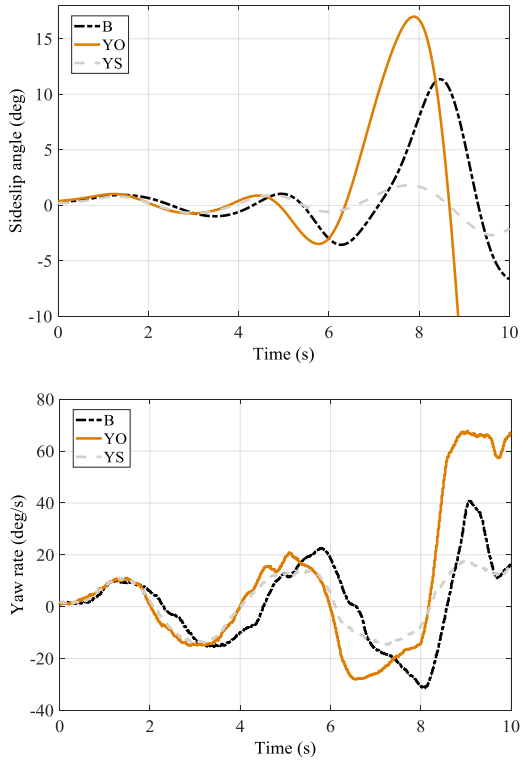

Fig. 6. Experimental slalom maneuver. Time histories of: a) sideslip angle; and b) yaw rate, for the baseline vehicle (B), the vehicle with the TV controller only based on r_h (YO), and the vehicle with the proposed SISO yaw rate and sideslip controller (YS).

Fig. 7 reports the average slip angles of the front and rear axles. In particular, the front slip angle, α_{FA}, is calculated from the front sideslip angle and average steering angle of the two front wheels, δ, i.e., $\alpha_{FA} = \delta - \beta_{FA}$. The rear slip angle, α_{RA}, is equal in magnitude to β_{RA}, i.e., $\alpha_{RA} = -\beta_{RA}$. From 0 s to 4 s, α_{FA} tends to be larger in magnitude than α_{RA} for all cases, i.e., the vehicle understeers. After 4 s, the B and YO vehicles present a rear slip angle significantly larger (in magnitude) than the front slip angle, i.e., they show an oversteering behavior, differently from the YS vehicle.

Five objective performance indicators are adopted for the assessment of each vehicle set-up:

- The root mean square value of the yaw rate error, $RMSE$, which assesses the tracking performance of

the feedback controller on yaw rate:

$$RMSE = \sqrt{\frac{1}{t_f - t_i}\int_{t_i}^{t_f}(r_{ref}(t) - r(t))^2 dt} \qquad (6)$$

where t_i and t_f represent the initial time and final time of the relevant part of the test, respectively. In particular, $t_f - t_i$ = 10 s for the specific tests.

- The maximum absolute value of sideslip angle at the rear axle, i.e., $|\beta_{RA,max}|$. Based on the analysis presented in Section 2, this corresponds to the maximum absolute value of the dynamic sideslip angle.
- The normalized integral of the absolute value of the control action, $IACA$, which evaluates the amount of direct yaw moment control effort:

$$IACA = \frac{1}{t_f - t_i}\int_{t_i}^{t_f}|M_z(t)|\,dt \qquad (7)$$

- $\Delta V\%$, which provides the magnitude of the vehicle speed reduction during the test, expressed as a percentage of the initial speed, V_m:

$$\Delta V\% = 100\frac{V_m - V(t_f)}{V_m} \qquad (8)$$

- The normalized integral of the absolute value of the steering wheel control action applied by the driver, $IASCA$. This indicator represents the steering wheel effort required for the successful completion of the test, i.e., for not hitting any cone:

$$IASCA = \frac{1}{t_f - t_i}\int_{t_i}^{t_f}|\delta(t)|\,dt \qquad (9)$$

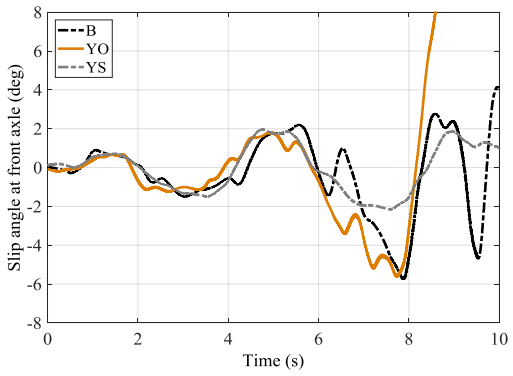

a)

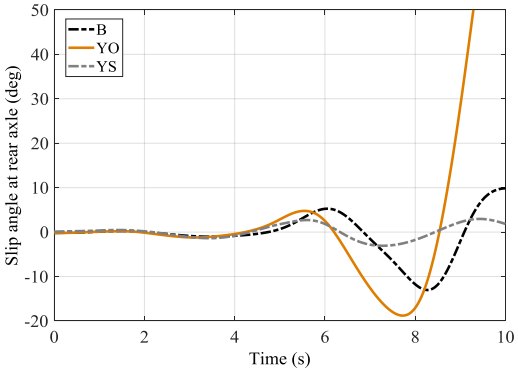

b)

Fig. 7. Experimental slalom maneuver. Time histories of: a) $\alpha_{FA}(t)$; and b) $\alpha_{RA}(t) = -\beta_{RA}(t)$, for the three vehicle set-ups.

Based on Table 1 and Fig. 6, the B vehicle has a very limited yaw rate tracking performance, simply because there is no yaw rate control. The maximum value of sideslip angle is significantly higher than a safety-critical acceptable value (approximately 4-5 deg); nevertheless, the driver was able to complete the maneuver. The YO vehicle is characterized by a large control effort; yet it is not able to follow the reference yaw rate (high $RMSE$), as it spins due to the high friction conditions assumed by the controller without sideslip-based correction. For the same reason, the steering effort and the reduction in vehicle speed are significant for the YO vehicle, worse than for the B vehicle. On the other hand, the YS vehicle guarantees the smallest $|\beta_{RA,max}|$, the best yaw rate tracking performance, the smallest vehicle speed reduction, and the lowest steering effort for the driver. Hence, the safety benefit achieved with the proposed controller is evident.

Table 1. Performance indicators for the experimental maneuver, V_m = 37 km/h.

Vehicle layout	$RMSE$ (deg/s)	$\lvert\beta_{RA,max}\rvert$ (deg)	$IACA$ (Nm)	$\Delta V\%$	$IASCA$ (deg)
B	17.9	13.0	0	21.3	54.4
YO	47.1	85.6	1224	56.1	87.8
YS	3.4	3.1	1013	5.2	29.0

5. CONCLUSION

The paper demonstrated that effective yaw rate control with appropriate constraints on sideslip angle is achievable with a SISO control formulation, i.e., with a simple yaw rate controller, in which the reference yaw rate is modified according to the measured or estimated sideslip angle. The proposed controller uses the sideslip angle at the rear axle, β_{RA}, as control variable, because it causes the sideslip-based intervention only when it is actually needed, i.e., when there is a significant dynamic sideslip angle. On the other hand, the adoption of the sideslip angle at the center of gravity or the front axle would imply interventions of the sideslip correction in conditions of large steering wheel inputs and trajectory curvatures. These correspond to large kinematic sideslip angle values, which do not necessarily result into safety-critical vehicle operation.

The simulation results show that the proposed controller significantly extends the stable region of vehicle operation on the $\dot{\beta}$-β phase-plane for high values of the tire-road friction coefficient. This means that sideslip control is beneficial also when the handling yaw rate is appropriately designed for the available friction level.

The controller was experimentally assessed on a vehicle prototype in varying and very low friction conditions. The vehicle with the TV controller operating with a reference cornering behavior designed for better tire-road friction conditions than those actually available generated more safety-critical conditions than the corresponding baseline vehicle. The tests with the proposed sideslip-based correction of the reference yaw rate showed consistently safe vehicle behavior, with significant improvements over the baseline vehicle and

the vehicle with the TV controller with a reference yaw rate for high friction conditions. Based on the experiments, in variable friction conditions it is more important to have appropriate and swiftly adaptable generation of the reference yaw rate signal, rather than an advanced control structure focused on providing excellent tracking performance.

ACKNOWLEDGEMENTS

The research leading to these results has received funding from the European Union Seventh Framework Programme FP7/2007-2013 under Grant Agreement No. 608897 (iCOMPOSE project).

REFERENCES

[1] Esmailzadeh, E., Goodarzi, A., Vossoughi, G.R., "Optimal yaw moment control law for improved vehicle handling," Mechatronics, 13(7), pp. 659-675, 2003.

[2] Kaiser, G., "Torque vectoring - linear parameter-varying control for an electric vehicle," PhD Thesis, Hamburg-Harburg Technical University, 2014.

[3] Tota, A., Lenzo, B., Lu, Q., Sorniotti, A., Gruber, P., Fallah, S., Velardocchia, M., Galvagno, E., De Smet, J., "On the experimental analysis of integral sliding modes for yaw rate and sideslip control," International Journal of Automotive Technology, 2018 (in press).

[4] Wang, Z., Montanaro, U., Fallah, S., Sorniotti, A., Lenzo, B., "A gain scheduled robust linear quadratic regulator for vehicle direct yaw moment control," Mechatronics, 51, pp. 31-45, 2018.

[5] De Novellis, L., Sorniotti, A., Gruber, P., "Driving modes for designing the cornering response of fully electric vehicles with multiple motors," Mechanical Systems and Signal Processing, 64-65, pp. 1-15, 2015.

[6] De Novellis, L., Sorniotti, A., Gruber, P., Pennycott, A, "Comparison of feedback control techniques for torque-vectoring control of fully electric vehicles," IEEE Transactions on Vehicular Technology, 63(8), pp. 3612-3623, 2014.

[7] Lenzo, B., Sorniotti, A., De Filippis, G., Gruber, P., Sannen, K., "Understeer characteristics for energy-efficient fully electric vehicles with multiple motors," International Battery, Hybrid and Fuel Cell Electric Vehicle Symposium (EVS29), 2016.

[8] Bucchi, F., Lenzo, B., Frendo, F., Sorniotti, A., De Nijs, W., "The effect of the front-to-rear wheel torque distribution on vehicle handling: an experimental assessment," 25th International Symposium on dynamics of vehicles on roads and tracks (IAVSD), 2017.

[9] Bucchi, F., Frendo, F., "A new formulation of the understeer coefficient to relate yaw torque and vehicle handling," Vehicle System Dynamics, 54(6), pp. 831-847, 2016.

[10] Liu, C.S., Peng, H., "Road friction coefficient estimation for vehicle path prediction," Vehicle system dynamics, 25(S1), pp. 413-425, 1996.

[11] Voser, C., Hindiyeh, R., Gerdes, J., "Analysis and control of high sideslip manoeuvres," Vehicle System Dynamics, 48(S1), pp. 317-336, 2010.

[12] Lenzo, B., Sorniotti, A., Gruber, P., Sannen, K., "On the experimental analysis of single input single output control of yaw rate and sideslip angle," International Journal of Automotive Technology, 18(5), pp. 799-811, 2017.

[13] Lu, Q., Gentile, P., Tota, A., Sorniotti, A., Gruber, P., Costamagna, F., De Smet, J., "Enhancing vehicle cornering limit through sideslip and yaw rate control," Mechanical Systems and Signal Processing, 75, pp. 455-472, 2016.

[14] Lenzo, B., De Filippis, G., Dizqah, A.M., Sorniotti, A., Gruber, P., Fallah, S., De Nijs, W., "Torque distribution strategies for energy-efficient electric vehicles with multiple drivetrains," Journal of Dynamic Systems, Measurement, and Control, 139(12), p. 121004, 2017.

[15] De Filippis, G., Lenzo, B., Sorniotti, A., Gruber, P., De Nijs, W., "Energy-efficient torque-vectoring control of electric vehicles with multiple drivetrains," IEEE Transactions on Vehicular Technology, 2018 (in press).

[16] Teng, G.W., Xiong, L., Leng, B., Hu, S.L., "A novel reference model for vehicle dynamics control," 24th International Symposium on Dynamics of Vehicles on Roads and Tracks (IAVSD), 2015.

[17] Guiggiani, M., "The science of vehicle dynamics: handling, braking, and ride of road and race cars," Springer, 2014.

[18] Genta, G., "Motor vehicle dynamics: modeling and simulation," World Scientific, 1997.

[19] Chindamo, D., Lenzo, B., Gadola, M. "On the vehicle sideslip angle estimation: a literature review of methods, models, and innovations," Applied Sciences, 8(3), p. 355, 2018.

[20] Farroni, F., Pasquino, N., Rocca, E., Timpone, F., "A comparison among different methods to estimate vehicle sideslip angle," World Congress on Engineering, 2015.

[21] Gadola, M., Chindamo, D., Romano, M., Padula, F., "Development and validation of a Kalman filter-based model for vehicle slip angle estimation," Vehicle System Dynamics, 52(1), pp. 68-84, 2014.

[22] Baffet, G., Charara, A., Stephant, J., "Sideslip angle, lateral tire force and road friction estimation in simulations and experiments," IEEE International Conference on Control Applications, 2006.

[23] Farroni, F., Russo, M., Russo, R., Terzo, M., Timpone, F., "A combined use of phase plane and handling diagram method to study the influence of tyre and vehicle characteristics on stability," Vehicle System Dynamics, 51(8), pp. 1265-1285, 2013.